Journal of the Korean Astronomical Society
54: 37 ∼ 47, 2021 April
https://doi.org/10.5303/JKAS.2021.54.2.37
pISSN: 1225-4614 · eISSN: 2288-890X
http://jkas.kas.org

Simulations of Torus Reverberation Mapping Experiments with SPHEREx

Minjin Kim[1], Woong-Seob Jeong[2,3], Yujin Yang[2,3], Jiwon Son[1], Luis C. Ho[4,5], Jong-Hak Woo[6,7], Myungshin Im[6,7], and Woowon Byun[2,3]

[1]Department of Astronomy and Atmospheric Sciences, College of Natural Sciences, Kyungpook National University, Daegu 41566, Korea; mkim.astro@gmail.com
[2]Korea Astronomy and Space Science Institute, Daejeon 34055, Korea
[3]University of Science and Technology, Daejeon 34113, Korea
[4]Kavli Institute for Astronomy and Astrophysics, Peking University, Beijing 100871, China
[5]Department of Astronomy, School of Physics, Peking University, Beijing 100871, China
[6]Astronomy Program, Department of Physics and Astronomy, Seoul National University, Seoul 08826, Korea
[7]SNU Astronomy Research Center, Seoul National University, Seoul 08826, Korea

Received August 24, 2020; accepted February 19, 2021

Abstract: Reverberation mapping (RM) is an efficient method to investigate the physical sizes of the broad line region (BLR) and dusty torus in an active galactic nucleus (AGN). The Spectro-Photometer for the History of the Universe, Epoch of Reionization and Ices Explorer (SPHEREx) mission will provide multi-epoch spectroscopic data at optical and near-infrared wavelengths. These data can be used for RM experiments with bright AGNs. We present results of a feasibility test using SPHEREx data in the SPHEREx deep regions for torus RM measurements. We investigate the physical properties of bright AGNs in the SPHEREx deep field. Based on this information, we compute the efficiency of detecting torus time lags in simulated light curves. We demonstrate that, in combination with complementary optical data with a depth of ~ 20 mag in $B-$band, lags of ≤ 750 days for tori can be measured for more than ~ 200 bright AGNs. If high signal-to-noise ratio photometric data with a depth of $\sim$ 21–22 mag are available, RM measurements are possible for up to ~ 900 objects. When complemented by well-designed early optical observations, SPHEREx can provide a unique dataset for studies of the physical properties of dusty tori in bright AGNs.

Key words: black hole physics — galaxies: active — galaxies: Seyfert — quasars: general — infrared: galaxies — dust — surveys

1. Introduction

An active galactic nucleus (AGN) is believed to originate from the strong thermal/non-thermal emission generated from the accretion disk around a supermassive black hole (SMBH) at the center of a galaxy. Observational and theoretical studies suggested that SMBHs dominantly gain their mass from accreted gas during the bright AGN phase [Quasi-stellar Objects (QSO) phase]. Hence, knowledge of the AGN is essential for understanding the formation and evolution of an SMBH over cosmic time (e.g., Yu & Tremaine 2002). According to the AGN unification model (Antonucci 1993; Urry & Padovani 1995), the central region of an AGN is composed of an accretion disk around the SMBH, a broad line region (BLR), a dusty torus, and a narrow line region (NLR). Therefore, studies of the physical properties of these subcomponents are of great importance to understand the innermost structure of AGNs (e.g., Blandford & McKee 1982; López-Gonzaga et al. 2016; Gravity Collaboration 2020b).

Because the physical sizes of the central structures, except the NLR, are relatively small ($\leq$ a few pc), exploring their structures directly with high-resolution images has been limited to nearby AGNs (e.g., Jaffe et al. 2004; Gravity Collaboration 2020a,b). Therefore, the reverberation mapping (RM) method has been used widely to investigate the physical size of central structures (Blandford & McKee 1982). The UV/optical featureless continuum originates from the accretion disk, and the broad emission lines arise from the photoionization of the gas in the BLR by UV photons from the accretion disk. Therefore, the flux of the broad emission lines varies in response to variations in the optical continuum with a time delay. This time lag between the two components is a good indicator of the physical distance between the accretion disk and the BLR.

The RM method has been widely applied to measure the size of the BLR in AGNs. Using knowledge of the line width of the broad emission line along with RM can provide estimates of the mass of the SMBH by the virial method. Interestingly, the size of the BLR is reported to be strongly correlated with the luminosity of AGN, resulting in a characteristic size–luminosity relation (e.g., Kaspi et al. 2000; Bentz et al. 2013; Du et al. 2016). Using this correlation, one can estimate the BH mass even from a single-epoch spectrum with

Corresponding author: M. Kim

Table 1
Summary of observation strategies

Epoch	Optical Data		SPHEREx	
	Cadence1	Cadence2	Cadence	Sea. Gap
(1)	(2)	(3)	(4)	(5)
epoch1 (Opt2 + IR1)	1 month	2 weeks	6 days	6 months
epoch2 (Opt1 + IR1)	1 month	1 week	6 days	6 months
epoch3 (Opt2 + IR2)	1 month	2 weeks	6 days	9 months
epoch4 (Opt1 + IR2)	1 month	1 week	6 days	9 months

Columns: (1): Name of observing strategy. (2): Cadence of complementary optical data during the first 1.5 years. (3): Cadence of complementary optical data during the later 2.5 years. (4): Cadence of SPHEREx data. (5): Seasonal gap for SPHEREX data.

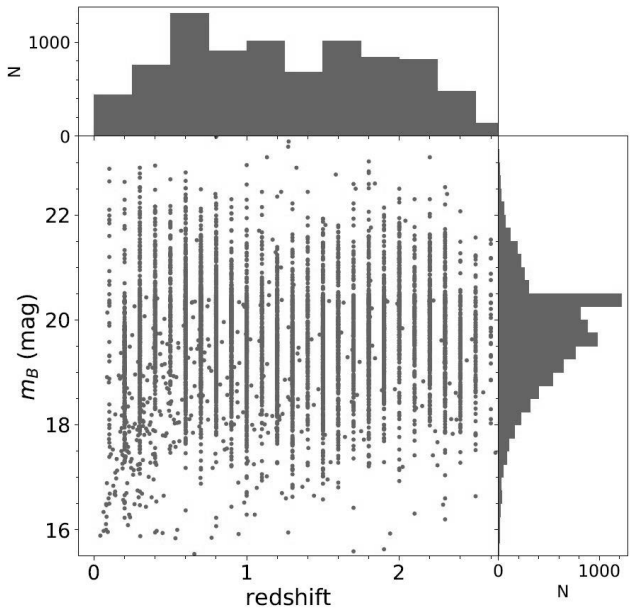

Figure 1. Distributions of redshift and $B-$band apparent magnitude (m_B) of target QSOs in the SPHEREx deep regions.

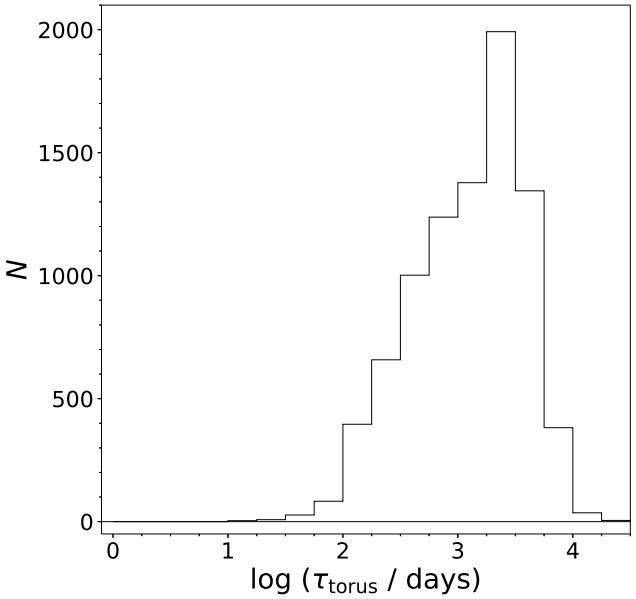

Figure 2. Predicted distributions of observed time lags for torus emission.

an uncertainty of $\sim$ 0.3–0.4 dex (Onken et al. 2004; Woo et al. 2010; Ho & Kim 2014). RM experiments require large amounts of observation time; hence, BLR time lags have been successfully measured for about a hundred AGNs so far (e.g., Peterson et al. 2004; Bentz et al. 2009; Barth et al. 2015; Kim et al. 2019; Rakshit et al. 2019). While on-going RM projects that utilize multi-object spectrographs can increase the sample size significantly, they are still insufficient to investigate the BLR properties for sufficiently wide ranges of various physical parameters of AGNs (e.g., Eddington ratio and black hole mass; King et al. 2015; Shen et al. 2015; Grier et al. 2017; Du et al. 2018; Shen et al. 2019).

The RM method can also be used to estimate the size of the dusty torus. The dust in the torus is heated by the UV emission from the accretion disk and radiates thermal energy mostly in the infrared (IR). Similar to observation in RM experiment with BLR, the time lag between IR and UV emission provides a constraint on the sublimation radius. Torus RM measurements are even more limited, to a few dozens of AGNs, because intensive IR monitoring with ground-based telescopes is a challenge (e.g., Clavel et al. 1989; Glass 2004; Koshida et al. 2014). Recently, the IR survey data from the Wide-field Infrared Survey Explorer (WISE; Wright et al. 2010) in combination with the optical photometric data from various transient surveys were successfully used in RM observations of tori (Lyu et al. 2019). However, the WISE multi-epoch data are obtained with a cadence of six months, resulting in relatively large uncertainties in the lag measurements for any given target.

The Spectro-Photometer for the History of the Universe, Epoch of Reionization and Ices Explorer (SPHEREx) mission will conduct an all-sky spectral imaging survey covering a spectral range of 0.75–4.5 μm with a 5σ depth of 19 mag[1] in each spectral bin (Dore et al. 2016, 2018). The mission is scheduled to be launched in late 2023 and perform all-sky mapping four times over the course of two years. It will employ linear variable filters to obtain spectral imaging data with a spectral

[1]This depth can be achieved with a single visit.

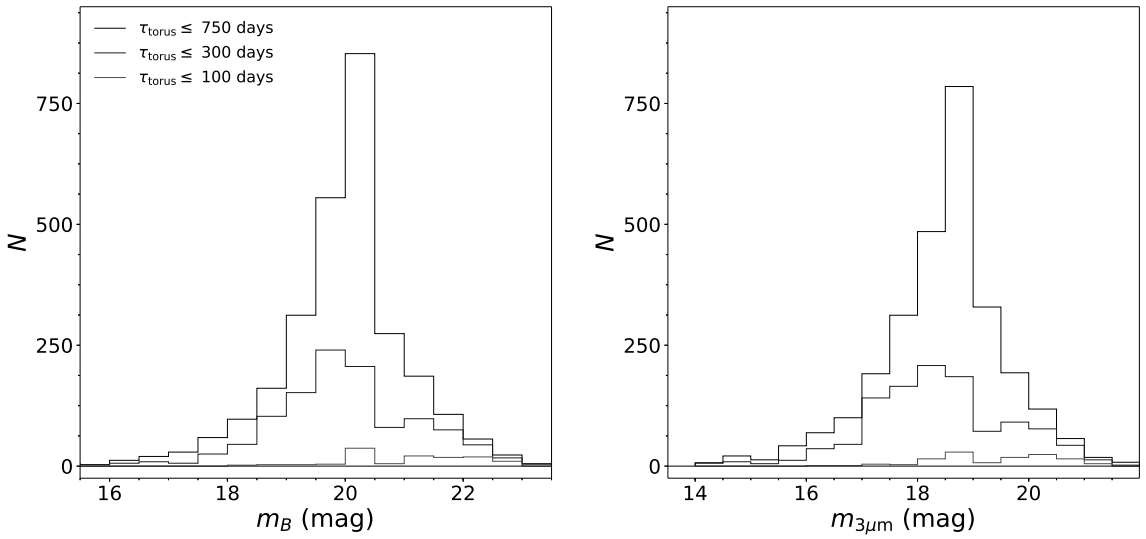

Figure 3. Distributions of the apparent magnitudes in $B-$band (left) and at 3 μm (right) of the primary targets (with $\tau_{\rm torus} \leq 750$ days). The IR brightness is computed using the QSO template from Hickox et al. (2017).

resolution of ~ 40. Because of its wide field of view, SPHEREx will cover the deep regions (~ 200 deg^2) around the equatorial poles more than 100 times in two years. The multi-epoch dataset in the deep survey fields will allow us to conduct RM experiments for both the BLRs and tori of selected AGNs, owing to the optical/NIR wavelength coverage and spectral capability. However, due to the relatively short baseline (about two years) of the SPHEREx mission, time lags larger than two years are not detectable solely with SPHEREx data. Therefore, early complementary optical monitoring is needed to increase the efficiency of detecting time lags in light curves of bright AGNs (Shen et al. 2015).

The goals of this work are (1) to explore the feasibility of *torus* RM measurements with the SPHEREx dataset and (2) to find the optimal way to obtain complementary optical data. BLR RM will be discussed elsewhere. The paper is organized as follows. In Section 2, we report a search for bright AGNs (i.e., QSOs) in the SPHEREx deep fields. In Section 3, we describe our methods to generate the simulated light curves. In Section 4, we present the results of RM measurements from the simulated light curves. In Section 5, we discuss the best way to maximize the efficiency of the RM experiments. Throughout this paper, we have adopted the following cosmological parameters: $H_0 = 100h = 67.8$ km s^{-1} Mpc^{-1}, $\Omega_{\rm m} = 0.308$, and $\Omega_\Lambda = 0.692$ (Planck Collaboration et al. 2016).

2. Sample Characteristics

It is vital to investigate the physical properties of target QSOs in SPHEREx deep fields around the north and south ecliptic poles from the two perspectives of testing the feasibility of the RM experiments and identifying the best strategy for obtaining complementary optical imaging data. In this context, the most essential properties are the brightness of the potential targets and expected time lags for the BLR and torus. To search for targets, we assume that the north and south deep fields are centered on R.A. = 17:55:24, Dec. = 66:37:32 and R.A. = 4:44:00, Dec. = $-$53:20:00, respectively. Each field covers 100 deg^2 within a radius of 5.64 degrees. Although the positions of the deep fields have not yet been determined, the statistical properties of target QSOs should not be sensitive to the exact positions, considering the wide area of the fields.

We use the Million Quasars (MILLIQUAS) Catalog, version 6.4 (Flesch 2019) to search for potential targets for RM studies. We find 5867 and 3674 QSOs in the north and south fields, respectively. Because those regions were not covered by large spectroscopic surveys such as the Sloan Digital Sky Survey (SDSS) and the 2dF and 6dF galaxy surveys, the majority of the sample comprises QSO *candidates* selected from multi-wavelength photometric data (e.g., WISE; Secrest et al. 2015), which are yet to be confirmed spectroscopically. The photometric redshifts of the QSO candidates were estimated based on optical and mid-infrared (MIR) colors (Flesch 2015). The uncertainty of these redshifts is approximately 50%.[2] Figure 1 shows the distributions of redshift and apparent magnitude in the $B-$band (m_B). Because the completeness of the MILLIQUAS catalog is unknown, we independently estimate the expected number of QSOs in the deep fields. Using the number counts of QSOs for $z < 2.1$ (Richards et al. 2005), at $m_B < 20$ mag, ~ 3500 QSOs are expected to be present in a field of 200 deg^2, while we find ~ 5600 objects in the MILLIQUAS catalog. Taking into account the predicted type 1 fraction ($\sim 50\%$; see below) in the sample, the two values appear broadly consistent.

In order to estimate expected time lags, we adopt the size–luminosity relation for the torus sublimation radius reported by Koshida et al. (2014), $R_{\rm sub} = -2.11 - 0.2 \times M_V$, where $R_{\rm sub}$ is the dust sublimation radius

[2] https://heasarc.gsfc.nasa.gov/W3Browse/all/milliquas.html

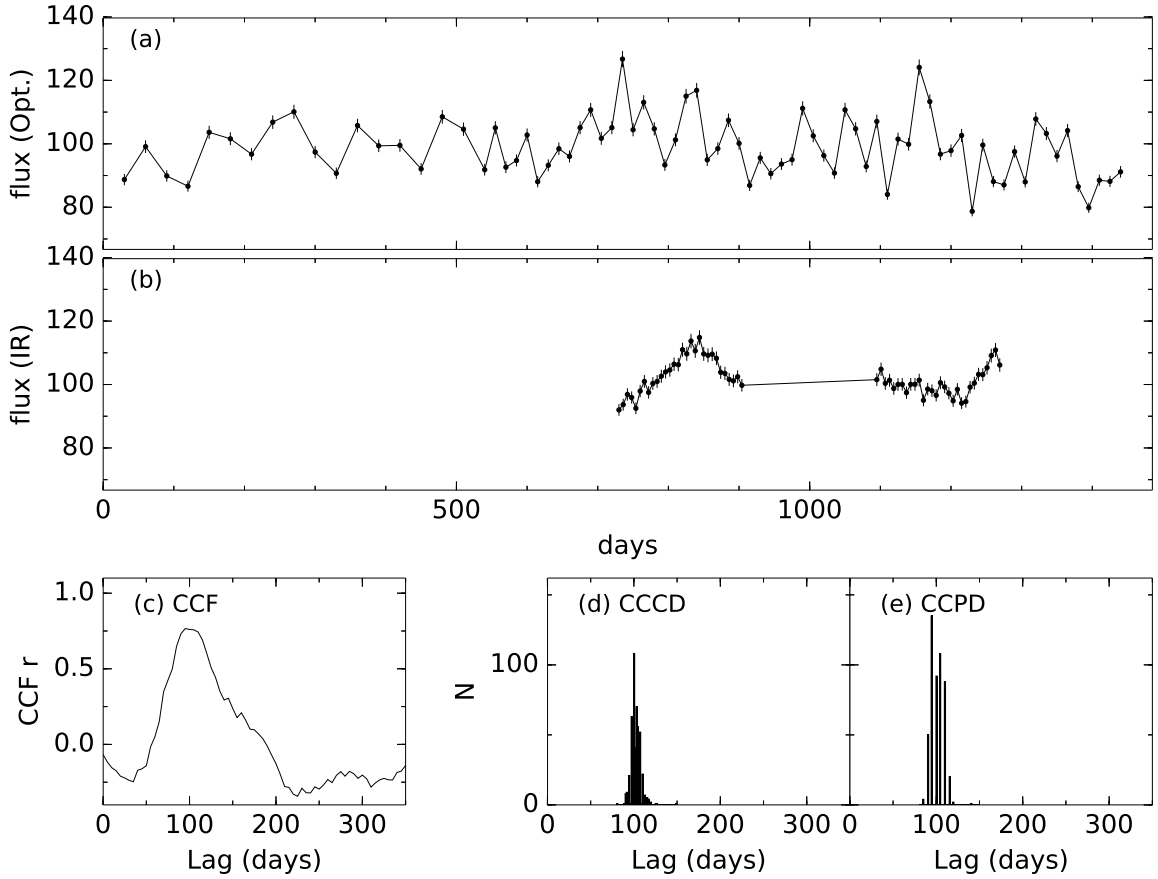

Figure 4. Examples of simulated light curves and time lag measurements using the interpolated cross correlation function (ICCF). The variability amplitude is 10%. The photometric error is set to 2% for both the optical and the IR band. The input time lag (true time lag) is 100 days. The measured time lag is $102.5^{+4.9}_{-4.9}$ days. (a) Optical light curve obtained with "Opt1". (b) IR light curve obtained with "IR1". (c) Cross correlation function (CCF), in which the cross-correlation Pearson coefficient (r) between the optical and IR light curves is shown as a function of time lag. (d) Cross-correlation centroid distribution (CCCD) estimated using Monte-Carlo iterations. The centroid of the time lag is computed using all cross-correlation coefficients above 80% of the peak value. We adopt the median of the CCCD as a proxy for the time lag because it is known to be less biased (Peterson et al. 2014). (e) Cross-correlation peak distribution (CCPD) estimated using Monte-Carlo iterations.

measured in the $K-$band in units of light days. We convert m_B to the monochromatic luminosity at 5100 Å, L_{5100}, and M_V using the optical/IR spectral template of QSOs (Hickox et al. 2017). Finally, we account for the cosmological time delay $(1+z)$ to estimate the time lags in the observer frame, $\tau_{\rm torus}$.

The predicted distribution of $\tau_{\rm torus}$ is presented in Figure 2. The uncertainty of ≈ 0.25 dex is introduced mainly by the lack of spectroscopic redshift data and the intrinsic scatter (≈ 0.13 dex) in the size–luminosity relations (Koshida et al. 2014). Assuming a two-year mission of SPHEREx, time lags larger than 750 days may not be detectable even in combination with optical imaging data obtained during the two years prior to the SPHEREx mission. Using the simulation described in Section 3, we confirm that time lags above two years are barely detected. Therefore, we consider QSOs with $\tau_{\rm torus}$ smaller than 750 days (~ 2 years) as the primary targets. Throughout the paper, only the primary targets are discussed. Overall, we found 2785 (1129) QSOs with $\tau_{\rm torus} \leq 750$ (300) days.

The fraction of type 1 sources among the IR-selected AGNs strongly depends on the bolometric luminosity (e.g., Assef et al. 2015). Therefore we compute the bolometric luminosity ($L_{\rm Bol}$) using L_{5100} and the bolometric conversion factor ($L_{\rm Bol} = 9.26 \times L_{5100}$; Richards et al. 2006). This yields $L_{\rm Bol}$ values from $10^{44.5-46}$ erg s^{-1} with a median value of $10^{45.4}$ erg s^{-1} for the primary targets. The type 1 AGN fraction is expected to vary from 0.3 to 0.7 (Equation 15 of Assef et al. 2015). For the sake of simplicity, we assume that half of the QSO candidates are of type 1.

Figure 3 shows the brightness distributions for the primary targets. We assume that the flux at 3 μm will be mainly used for the IR RM study, which approximately corresponds to the K-band in the rest frame of the target QSOs at the median redshift. Since for high-redshift targets the contamination from the accretion

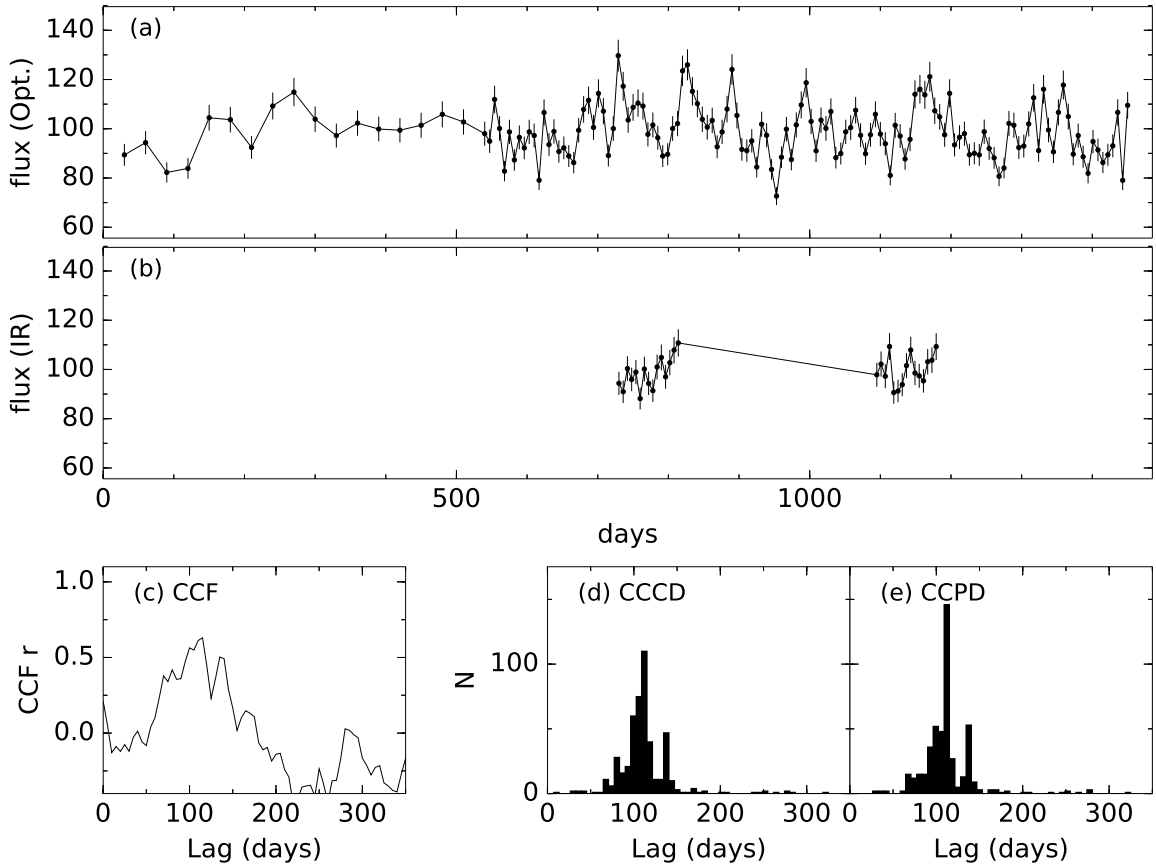

Figure 5. Same as Figure 4, except that the photometric error is set to 5% for both the optical and IR band; optical light curve obtained with "Opt2"; IR light curve obtained with "IR2". The estimated time lag is $110.1^{+27.4}_{-12.9}$ days.

disk may not be negligible even at 3 μm (Sakata et al. 2010; Koshida et al. 2014; Hönig 2014), we will make use of the flux at longer wavelength. In addition, thanks to the wide spectral coverage of the SPHEREx dataset, we will also investigate the color variation in NIR, which will provide useful constraints on the structure of the torus.

The AB magnitude at 3 μm is computed from m_B using the optical/IR QSO template of Hickox et al. (2017). Approximately 76% of the primary targets is expected to be brighter than 19 mag at 3 μm, indicating that the IR variability can be measured reliably by the SPHEREx survey. Furthermore, 19 mag at 3 μm approximately corresponds to 20 mag in the B-band. Therefore, optical imaging data to trace the UV/optical variability are necessary to reach 21–22 mag with a 5σ detection limit to maximize the sample size. The QSOs fainter than 19 mag can be used for the RM study after increasing the signal-to-noise ratio (S/N) through temporal or spectral binning. Spectral binning will be performed mainly within 9 or 10 spectral bins ($3\pm0.4\mu$m), in order to minimize the contamination from the accretion disk and preserve the color information. Overall, taking into account the type 1 fraction of $\sim$ 50%, we found that a sufficiently large sample of QSOs ($\sim$ 1400 sources) is available in the SPHEREx deep fields and can be used for RM measurements. These data will allow us to explore the central structure of QSOs comprehensively.

3. Simulations

3.1. Light Curves

To test the feasibility of RM experiments in the SPHEREx deep fields, we perform extensive simulations using artificial AGN light curves. In general, the power spectrum of AGN light curves can be modeled with a broken power law (Mushotzky et al. 2011; Kasliwal et al. 2015; Caplar et al. 2017) such that the the power spectrum at low frequencies is moderately flat, and that above the break frequency is steep. Here, we adopt the damped random walk (DRW) model to generate the light curves, which is known to well represent the observed light curve of bright AGNs (MacLeod et al. 2012). With spectral power scaling like $\propto \nu^{-\gamma}$, we assume $\gamma = 2$ at high frequencies and $\gamma = 0$ at low frequencies. While the break period ranges from 10 to 150 days, we assume a break period of 100 days in the simulation for the sake of simplicity (see also Woo et al. 2019).

The variability amplitude is generally known to be $\sim$ 10% in the optical band for bright QSOs (e.g., Giveon et al. 1999; Sánchez-Sáez et al. 2018). Therefore we

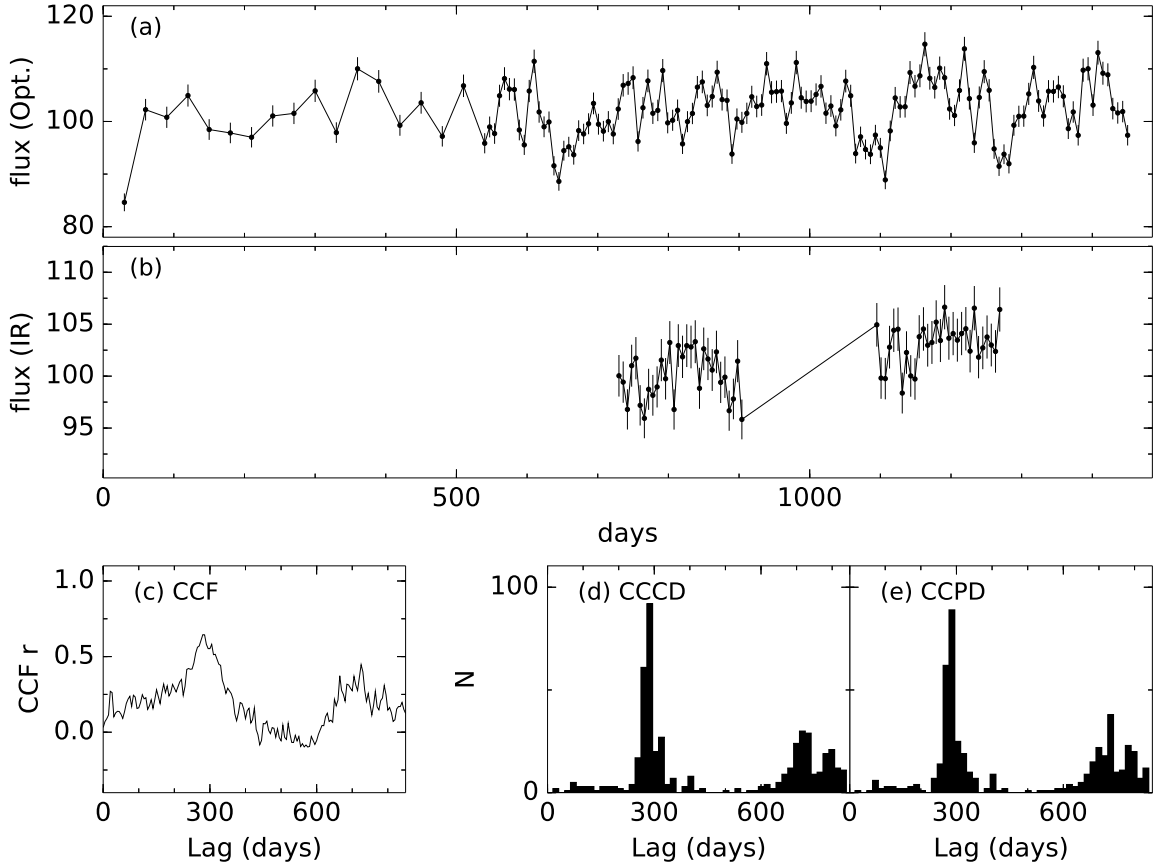

Figure 6. Same as Figure 4, except that the variability amplitude is 5%; optical light curve obtained with "Opt2"; the input time lag is 300 days. The estimated time lag is $295.1^{+319.9}_{-45.4}$ days.

assume that the variability amplitude is 10%. Several studies claimed that the variability amplitude increases with decreasing AGN luminosity (e.g., Sánchez-Sáez et al. 2018). Our sample comprises relatively faint QSOs ($43 \leq \log(L_{5100}/\mathrm{ergs}^{-1}) \leq 45$), suggesting that our assumption for the variability amplitude is conservative. However, the amplitude in the IR is significantly smaller than that in the optical band (Lyu et al. 2019). In addition, owing to the low spatial resolution of SPHEREx (~ 6 arcsec), light contamination from the host galaxy is of importance. Using high resolution images of nearby QSOs obtained with the Hubble Space Telescope (Kim et al. 2017), we find that the host brightness is comparable to the nuclear brightness on average, indicating that the variability amplitude can be reduced by $\sim 25\%$. In order to take these effects into account, we examine two cases (5% and 10% variability amplitude) for generating the artificial light curves. To investigate the dependence on the brightness of the targets, we artificially added photometric uncertainties ranging from 1% to 10% of the original flux. To assess the impact of different time lags, we consider three different lags: 100, 300, and 700 days. Because our goal is to demonstrate the general feasibility of the IR RM experiment with SPHEREx and to offer the best strategy, we simply assume that the variability amplitude and photometric uncertainty are the same for both the optical and IR bands in this experiment.

3.2. Observation Strategy

The success rate of time lag measurements is very sensitive to the observing epochs and the monitoring cadences. Therefore, we use two observing sequences for each of the complementary optical imaging data and IR spectroscopic data obtained from SPHEREx. To improve on the relatively short baseline of the SPHEREx mission (~ 2 years), optical monitoring data from ground-based telescopes are assumed to be obtained over four years, starting two years prior to the beginning of SPHEREx mission and continuing throughout the duration of the mission. In the first scenario (called "Opt1" throughout this paper), the data have a cadence of one month for the first 1.5 years, and one week for the remaining 2.5 years in order to detect shorter time lags. In the second scenario (called "Opt2"), the optical data are obtained with a cadence of two weeks over the last 2.5 years.

Because the mapping strategy for the SPHEREx survey has not been determined yet, we conservatively assume that IR multi-epoch data will be obtained with seasonal gaps and a cadence of six days for two years. We adopt two observing scenarios, namely, "IR1" with a seasonal gap of six months and "IR2" with a seasonal gap

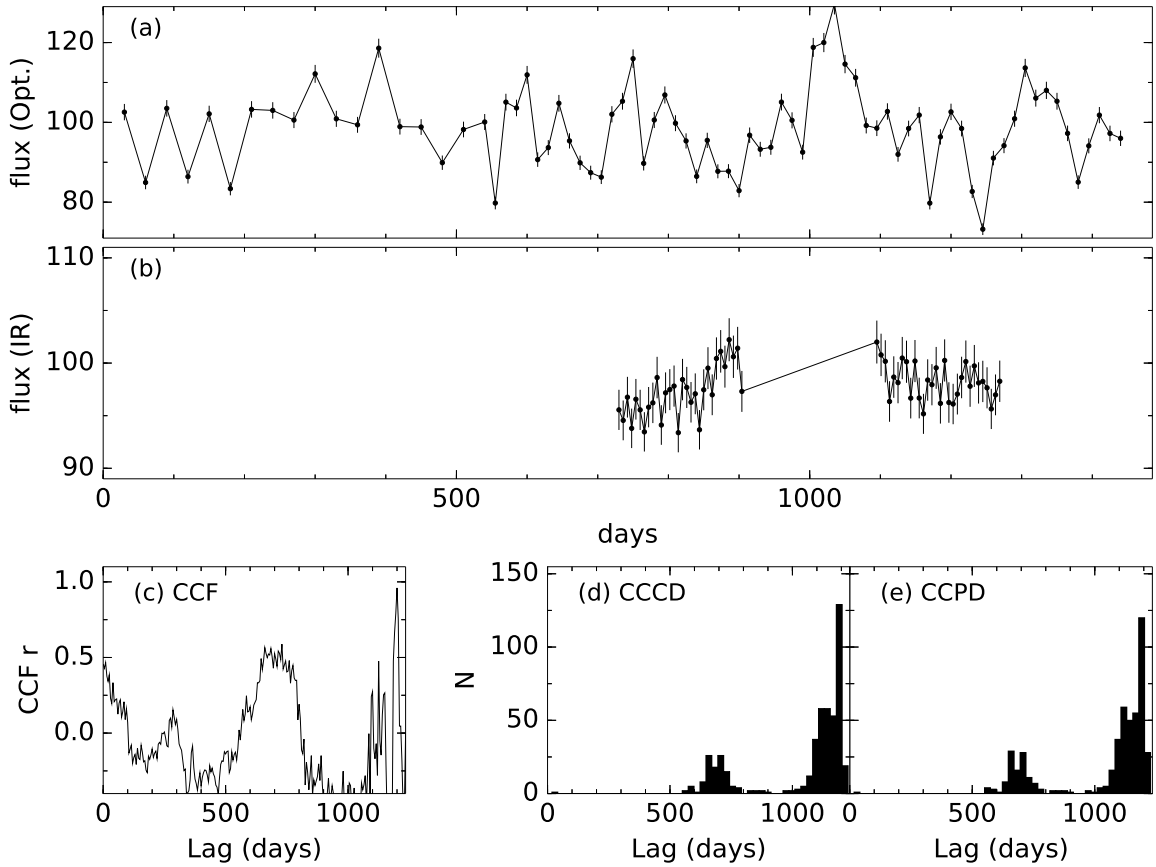

Figure 7. Same as Figure 4, except that the input time lag is 700 days. The estimated time lag is $1127.7^{+67.3}_{-414.8}$ days.

of nine months. While the IR1 mode may be applicable to the central part of the deep fields, the outer part can be more likely described by the IR2 mode. By combining the two scenarios of each observation (optical and IR), four different observing strategies are tested in this simulation (Table 1). We randomly generated 200 pairs of light curves at each position in a grid spanned by four parameters: observed time lag, observing strategy, variability amplitude, and photometric error.

The IR light curves are convolved with a top-hat transfer function to take into account the geometric effect of the dusty torus (Blandford & McKee 1982; Almeyda et al. 2020). The width ($d\tau$) of the top-hat function is set to be half of the time lag, with a maximum value of 200 days (Lyu et al. 2019).

4. Results

To estimate the efficiency of detecting the time lags between the simulated light curves, we use the interpolated cross correlation function (ICCF; Peterson et al. 1998) The errors of the measured time lag values are estimated by means of Monte Carlo simulations that use randomly drawn subsets of photometric data from the simulated light curves (Gaskel & Peterson 1987). The python code `PyCCF` (Sun et al. 2018) is utilized for this calculation. Prior to the time lag estimation, the optical light curves are convolved with the top-hat function previously applied to the IR light curves. We assume that a time lag has been recovered successfully if the measured value is within 10% of the input value. Examples of time lag measurements along with the corresponding light curves are shown in Figures 4–7.

The simulation results are summarized in Table 2. In most cases, the detection rate for epoch1 (epoch2) is significantly larger than that for epoch3 (epoch4) by up to 40%, showing that the seasonal gaps in the IR observation have a strong impact. However, we find little difference ($< 5\%$) between epoch1 (epoch3) and epoch2 (epoch4). This finding indicates that the cadence in the optical monitoring data is less important.

Figure 8 shows the detection efficiency for the time lags in light curves with 10% variability amplitude. The detection rates are higher than 50% for time lags of less than 300 days if the photometric error is smaller than 2%. Time lags larger than 300 days are recovered for less than half of all targets if the photometric error is larger than 2%. The detection rate dramatically decreases with increasing photometric error, demonstrating that high-S/N photometric data are essential for the precise measurement of time lags. Therefore, the S/N for faint targets ($m_{3\mu m} > 19$ mag) should be enhanced through spectral and temporal binning. This requirement also needs to be taken into account for the optical observations.

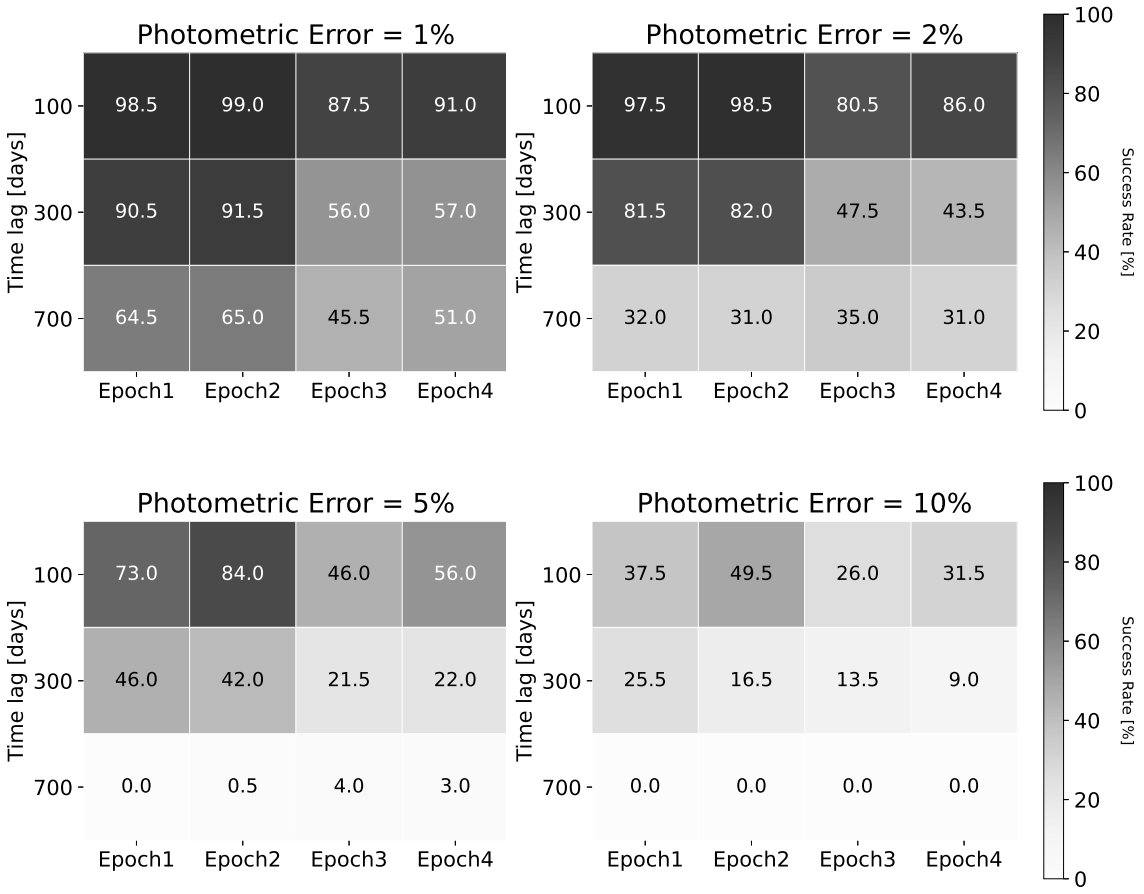

Figure 8. Efficiency of detecting time lags, for a variability amplitude of 10%, as function of input time lag and monitoring schedule. The detection rates are noted in each bin.

Overall, for a variability amplitude of $\sim 10\%$, the detection efficiency is relatively large if the photometric error is less than 5%. By multiplying the time lag distribution of the primary targets with the interpolated success rate, we expect successful time lag measurements for ~ 500 objects, a proper observation strategy (i.e., 5% photometric error and 10% variability amplitude) provided. If high S/N (i.e., 2% photometric error) optical monitoring data are available, time lags can be successfully measured for up to ~ 900 objects.

To take into account the variability amplitude in IR is smaller than that in the optical band, as well as the light contamination from the host galaxy, we perform the same experiments under the assumption of a variability amplitude of 5%. The results are shown in Figure 9. The success rate is significantly lower than for the case of a variability amplitude of 10%. Not surprisingly, it is almost impossible to detect large time lags (~ 300 days) if the photometric error is larger than the intrinsic variability amplitude (5%). However, in this worst case scenario (5% photometric error and 5% intrinsic variability), we may still be able to measure time lags for ~ 200 targets.

5. COMPLEMENTARY OPTICAL OBSERVATIONS

From our simulations we find that high-SN photometric data are the most important factor for a successful RM experiment, whereas the monitoring cadence is less important. Through spectral and temporal binning, we can achieve S/N > 10 for 19 mag at 3 μm. This approximately corresponds to 20 mag in the $B-$band. To maximize the sample size, it is therefore desirable that optical monitoring data reach to $\sim$21–22 mag in the $B-$band. Existing and planned optical transient surveys can be used for this purpose. For example, the Zwicky Transient Facility (ZTF) survey has a limiting magnitude of ~ 20.8 mag in the $g-$band (Bellm et al. 2019), which corresponds to ~ 21.5 mag in the $B-$band for typical QSOs (Richards et al. 2002; Lupton 2005). Because its average cadence is ~ 3 days, we can reach ~ 22 mag by combining it with other multi-epoch datasets. Indeed, the Large Synoptic Survey Telescope (LSST) will provide data for the deep region around SEP with a limiting magnitude of ~ 24.8 mag in $g-$band with a single visit (Ivezić et al. 2019). If public surveys are unavailable, optical monitoring observations should be executed using 1–2 meter class telescopes equipped with wide field of

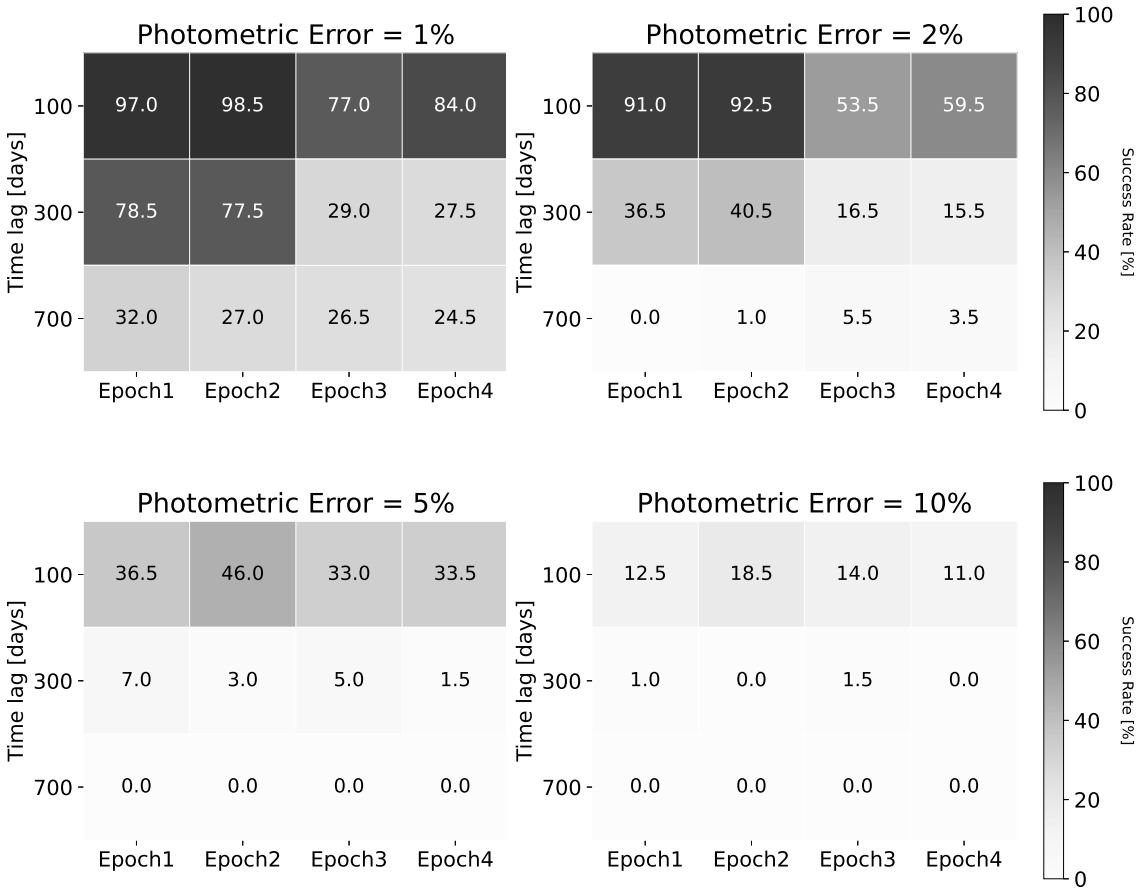

Figure 9. Same as Figure 8, but for a variability amplitude of 5%.

view cameras, such as the Korea Microlensing Telescope Network (KMTNet; Kim et al. 2016).

With well-designed complementary optical observations (e.g., with 5% photometric error at 20 mag[3]), one may be able to detect time lags for 200–500 objects, depending on the intrinsic variability of the target QSOs. In addition, owing to the large sample size in the SPHEREx deep fields, one can estimate a composite lag by stacking photometric data from individual targets (e.g., Fine et al. 2012; Li et al. 2017). On the other hand, previous studies on IR RM with a large sample relied on the WISE survey (Lyu et al. 2019; Yang et al. 2020), in which the IR data were obtained with a cadence of six months. Because the SPHEREx survey will be conducted with a much higher cadence (of about a few days) than WISE, the accuracy of the measurement for short (less than a couple of hundred days) time lags may be expected to be improved. IR RM studies with high cadence ground-based observations have been conducted for nearby AGNs (Koshida et al. 2014; Minezaki et al. 2012). The SPHEREx survey will provide high-S/N IR data for an unbiased large sample of AGNs at moderate redshifts, complementary to previous studies.

[3]Which is the median B-band magnitude of the primary targets.

6. Conclusions

In order to test the feasibility of RM experiments with SPHEREx data, we search for target QSOs in the SPHEREx deep regions and estimate the expected time lags in their light curves using the size–luminosity relations. We find that there are more than 1400 QSOs with $\tau_{\rm torus} \leq 750$ days which is suitable for RM studies. We simulate simulate AGN light curves to investigate the reliability of RM measurements; we find that the time lags can be measured for 200–500 objects depending on observation strategy (cadences and seasonal gaps) and photometric accuracies. In combination with complementary optical observations, RM studies with SPHEREx can provide a unique dataset for studies of the physical properties of the central structures of bright QSOs.

Acknowledgments

We are grateful to the anonymous reviewers for their critical reviews that greatly helped to improve our manuscript. This research was supported by the Kyungpook National University Research Fund, 2018.

Table 2
Success rates of simulated RM measurements

Time lag	Var.	Epoch	Photometric Error			
(days)			1%	2%	5%	10%
(1)	(2)	(3)	(4)	(5)	(6)	(7)
100	10%	epoch1	98.5	97.5	73.0	37.5
100	10%	epoch2	99.0	98.5	84.0	49.5
100	10%	epoch3	87.5	80.5	46.0	26.0
100	10%	epoch4	91.0	86.0	56.0	31.5
300	10%	epoch1	90.5	81.5	46.0	25.5
300	10%	epoch2	91.5	82.0	42.0	16.5
300	10%	epoch3	56.0	47.5	21.5	13.5
300	10%	epoch4	57.0	43.5	22.0	9.0
700	10%	epoch1	64.5	32.0	0.0	0.0
700	10%	epoch2	65.0	31.0	0.5	0.0
700	10%	epoch3	45.5	35.0	4.0	0.0
700	10%	epoch4	51.0	31.0	3.0	0.0
100	5%	epoch1	97.0	91.0	36.5	12.5
100	5%	epoch2	98.5	92.5	46.0	18.5
100	5%	epoch3	77.0	53.5	33.0	14.0
100	5%	epoch4	84.0	59.5	33.5	11.0
300	5%	epoch1	78.5	36.5	7.0	1.0
300	5%	epoch2	77.5	40.5	3.0	0.0
300	5%	epoch3	29.0	16.5	5.0	1.5
300	5%	epoch4	27.5	15.5	1.5	0.0
700	5%	epoch1	32.0	0.0	0.0	0.0
700	5%	epoch2	27.0	1.0	0.0	0.0
700	5%	epoch3	26.5	5.5	0.0	0.0
700	5%	epoch4	24.5	3.5	0.0	0.0

Columns: (1): Input time lag. (2): Variability amplitude. (3): Name of the observing strategy. (4): Success rate for 1% photometric error. (5): Success rate for 2% photometric error. (6): Success rate for 5% photometric error. (7): Success rate for 10% photometric error.

REFERENCES

Almeyda, T., Robinson, A., Richmond, M., Nikutta, R. & McDonough, B. 2020, Modeling the Infrared Reverberation Response of the Circumnuclear Dusty Torus in AGNs: An Investigation of Torus Response Functions, ApJ, 891, 26

Antonucci, R. 1993, Unified Models for Active Galactic Nuclei and Quasars, ARA&A, 31, 473

Assef, R. J., Eisenhardt, P. R. M., Stern, D., et al. 2015, Half of the Most Luminous Quasars May Be Obscured: Investigating the Nature of WISE-Selected Hot Dust-Obscured Galaxies, ApJ, 804, 27

Barth, A. J., Bennert, V. N., Canalizo, G., et al. 2015, The Lick AGN Monitoring Project 2011: Spectroscopic Campaign and Emission-line Light Curves, ApJS, 217, 26

Bellm, E. C., Kulkarni, S. R., Graham, M. J., et al. 2019, The Zwicky Transient Facility: System Overview, Performance, and First Results, PASP, 131, 018002

Bentz, M. C., Walsh, J. L., Barth, A. J., et al. 2009, The Lick AGN Monitoring Project: Broad-line Region Radii and Black Hole Masses from Reverberation Mapping of Hβ, ApJ, 705, 199

Bentz, M. C., Denney, K. D., Grier, Catherine J., et al. 2013, The Low-luminosity End of the Radius-Luminosity Relationship for Active Galactic Nuclei, ApJ, 767, 149

Blandford, R. D. & McKee, C. F. 1982, Reverberation Mapping of the Emission Line Regions of Seyfert Galaxies and Quasars, ApJ, 255, 419

Caplar, N., Lilly, S, J., & Trakhtenbrot, B. 2017, Optical Variability of AGNs in the PTF/iPTF Survey, ApJ, 834, 111

Clavel, J., Wamsteker, W., & Glass, I. S. 1989, Hot Dust on the Outskirts of the Broad-Line Region in Fairall 9, ApJ, 337, 236

Doré, O., Werner, M. W., Ashby, M., et al. 2016, Science Impacts of the SPHEREx All-Sky Optical to Near-Infrared Spectral Survey: Report of a Community Workshop Examining Extragalactic, Galactic, Stellar and Planetary Science, arXiv:1606.07039

Doré, O., Werner, M. W., Ashby, M., et al. 2018, Science Impacts of the SPHEREx All-Sky Optical to Near-Infrared Spectral Survey II: Report of a Community Workshop on the Scientific Synergies Between the SPHEREx Survey and Other Astronomy Observatories, arXiv:1805.05489

Du, P., Lu, K.-X., Zhang, Z.-X., et al. 2016, Supermassive Black Holes with High Accretion Rates in Active Galactic Nuclei. V. A New Size-Luminosity Scaling Relation for the Broad-line Region, ApJ, 825, 126

Du, P., Zhang, Z.-X., Wang, K., et al. 2018, Supermassive Black Holes with High Accretion Rates in Active Galactic Nuclei. IX. 10 New Observations of Reverberation Mapping and Shortened Hβ Lags, ApJ, 856, 6

Fine, S., Shanks, T., Croom, S. M., et al. 2012, Composite Reverberation Mapping, MNRAS, 427, 2701

Flesch, E. W. 2015, The Half Million Quasars (HMQ) Catalogue, PASA, 32, 10

Flesch, E. W. 2019, The Million Quasars (Milliquas) Catalogue, v6.4, arXiv:1912.05614

Gaskell, C. M., & Peterson, B. M. 1987, The Accuracy of Cross-Correlation Estimates of Quasar Emission-Line Region Sizes, ApJS, 65, 1

Giveon, U., Maoz, D., Kaspi, S., et al. 1999, Long-term Optical Variability Properties of the Palomar-Green Quasars, MNRAS, 306, 637

Glass, I. S. 2004, Long-term Infrared Photometry of Seyferts, MNRAS, 350, 1049

GRAVITY Collaboration (Dexter, J., et al.) 2020, The Resolved Size and Structure of Hot Dust in the Immediate Vicinity of AGN, A&A, 634, A92

GRAVITY Collaboration (Pfuhl, O., et al.) 2020, An Image of the Dust Sublimation Region in the Nucleus of NGC 1068, A&A, 634, A1

Grier, C. J., Trump, J. R., Shen, Y., et al. 2017, The Sloan Digital Sky Survey Reverberation Mapping Project: Hα and Hβ Reverberation Measurements from First-year Spectroscopy and Photometry, ApJ, 851, 21

Hickox, R. C., Myers, A. D., Greene, J. E., et al. 2017, Composite Spectral Energy Distributions and Infrared-Optical Colors of Type 1 and Type 2 Quasars, ApJ, 849, 53

Ho, L. C. & Kim, M. 2014, The Black Hole Mass Scale of Classical and Pseudo Bulges in Active Galaxies, ApJ, 789, 17

Hönig, S. F. 2014, Dust Reverberation Mapping in the Era of Big Optical Surveys and its Cosmological Application, ApJL, 784, L4

Ho, L. C. & Kim, M. 2014, The Black Hole Mass Scale of Classical and Pseudo Bulges in Active Galaxies, ApJ, 789, 17

Ivezić, Ž., Kahn, S, M., Tyson, J. A., et al. 2019, LSST: From

Science Drivers to Reference Design and Anticipated Data Products, ApJ, 873, 111
Jaffe, W., Meisenheimer, K., Röttgering, H. J. A., et al. 2004, The Central Dusty Torus in the Active Nucleus of NGC 1068, Nature, 429, 47
Kasliwal, V. P., Vogeley, M, S., & Richards, G, T. 2015, Are the Variability Properties of the Kepler AGN Light Curves Consistent with a Damped Random Walk?, MNRAS, 451, 4328
Kaspi, S., Smith, P. S., Netzer, H., et al. 2000, Reverberation Measurements for 17 Quasars and the Size–Mass–Luminosity Relations in Active Galactic Nuclei, ApJ, 533, 631
Kim, J., Im, M., Choi, C., et al. 2019, Medium-band Photometry Reverberation Mapping of Nearby Active Galactic Nuclei, ApJ, 884, 103
Kim, M.. Ho, L. C., Peng, C. Y., et al. 2017, Stellar Photometric Structures of the Host Galaxies of Nearby Type 1 Active Galactic Nuclei, ApJS, 232, 21
Kim, S.-L., Lee, C.-U., Park, B.-G., et al. 2016, KMTNET: A Network of 1.6 m Wide-Field Optical Telescopes Installed at Three Southern Observatories, JKAS, 49, 37
King, A. L., Martini, P., Davis, T. M., et al. 2015, Simulations of the OzDES AGN Reverberation Mapping Project, MNRAS, 453, 1701
Koshida, S., Minezaki, T., Yoshii, Y. et al. 2014, Reverberation Measurements of the Inner Radius of the Dust Torus in 17 Seyfert Galaxies, ApJ, 788, 159
Li, J., Shen, Y., Horne, K. et al. 2017, The Sloan Digital Sky Survey Reverberation Mapping Project: Composite Lags at $z \leq 1$, ApJ, 846, 79
López-Gonzaga, N., Burtscher, L., Tristram, K. R. W., Meisenheimer, K., & Schartmann, M. 2016, Mid-infrared Interferometry of 23 AGN Tori: On the Significance of Polar-elongated Emission, A&A, 591, A47
Lupton, R. H. 2005, SDSS Data Release 14, Transformations between SDSS Magnitudes and Other Systems, `http://www.sdss.org/dr14/algorithms/sdssUBVRITransform#Lupton2005`
Lyu, J., Rieke, G. H., & Smith, P. S. 2019, Mid-IR Variability and Dust Reverberation Mapping of Low-z Quasars. I. Data, Methods, and Basic Results, 2019, 886, 33
MacLeod, C. L., Ivezić, Ž, Sesar, B., et al. 2012, A Description of Quasar Variability Measured Using Repeated SDSS and POSS Imaging, ApJ, 753, 106
Minezaki, T., Yoshii, Y., Kobayashi, Y., et al. 2019, Reverberation Measurements of the Inner Radii of the Dust Tori in Quasars, ApJ, 886, 150
Mushotzky, R. F., Edelson, R., Baumgartner, W., et al. 2011, Kepler Observations of Rapid Optical Variability in Active Galactic Nuclei, ApJL, 743, L12
Onken, C. A., Ferrarese, L., Merritt, D., et al. 2004, Supermassive Black Holes in Active Galactic Nuclei. II. Calibration of the Black Hole Mass-Velocity Dispersion Relationship for Active Galactic Nuclei, ApJ, 615, 645
Peterson, B. M., Wanders, I., Horne, K., et al. 1998, On Uncertainties in Cross-Correlation Lags and the Reality of Wavelength-dependent Continuum Lags in Active Galactic Nuclei, PASP, 748, 660
Peterson, B. M., Ferrarese, L., Gilbert, K. M., et al. 2004, Central Masses and Broad-Line Region Sizes of Active Galactic Nuclei. II. A Homogeneous Analysis of a Large Reverberation-Mapping Database, ApJ, 613, 682
Peterson, B. M., Grier, C. J., Horne, K., et al. 2014, Reverberation Mapping of the Seyfert 1 Galaxy NGC 7469, ApJ, 795, 149
Planck Collaboration, Ade, P. A. R., Aghanim, N., et al. 2016, Planck 2015 results. XIII. Cosmological parameters, A&A, 594, 13
Rakshit, S., Woo, J.-H., Gallo, E., et al. 2019, The Seoul National University AGN Monitoring Project. II. BLR Size and Black Hole Mass of Two AGNs, ApJ, 886, 93
Richards, G. T., Croom, S. M., Anderson, S. F., et al. 2005, The 2dF-SDSS LRG and QSO (2SLAQ) Survey: The $z < 2.1$ Quasar Luminosity Function from 5645 Quasars to $g = 21.85$, MNRAS, 360, 839
Richards, G. T., Fan, X., Newberg, H. J., et al. 2002, Spectroscopic Target Selection in the Sloan Digital Sky Survey: The Quasar Sample, AJ, 123, 2945
Richards, G. T., Lacy, M., Storrie-Lombardi, L. J., et al. 2006, Spectral Energy Distributions and Multiwavelength Selection of Type 1 Quasars, ApJS, 166, 470
Sakata, Y., Minezaki, T., Yoshii, Y., et al. 2010, Long-Term Optical Continuum Color Variability of Nearby Active Galactic Nuclei, ApJ, 711, 461
Sánchez-Sáez, P., Lira, P., Mejía-Restrepo, J., et al. 2018, The QUEST-La Silla AGN Variability Survey: Connection between AGN Variability and Black Hole Physical Properties, ApJ, 864, 87
Secrest, N. J., Dudik, R. P., Dorland, B. N., et al. 2015, Identification of 1.4 Million Active Galactic Nuclei in the Mid-Infrared using WISE Data, ApJS, 221, 12
Shen, Y., Brandt, W. N., Dawson, K. S., et al. 2015, The Sloan Digital Sky Survey Reverberation Mapping Project: Technical Overview, ApJS, 216, 4
Shen, Y., Hall, P. B., Horne, K., et al. 2019, The Sloan Digital Sky Survey Reverberation Mapping Project: Sample Characterization, ApJS, 241, 34
Sun, M., Grier, C. J., & Peterson, B. M. 2018, PyCCF: Python Cross Correlation Function for Reverberation Mapping Studies, `ascl:1805.032`
Urry, C. M., & Padovani, P. 1995, Unified Schemes for Radio-Loud Active Galactic Nuclei, PASP, 107, 803
Woo, J.-H., Son, D., & Gallo, E., et al. 2019, Seoul National University AGN Monitoring Project. I. Strategy and Sample, JKAS, 52, 109
Woo, J.-H., Treu, T., Barth, A. J., et al. 2010, The Lick AGN Monitoring Project: The $M_{\rm BH}$–σ_* Relation for Reverberation-mapped Active Galaxies, ApJ, 716, 269
Wright, E. L., Eisenhardt, P. R. M., Mainzer, A. K., et al. 2010, The Wide-field Infrared Survey Explorer (WISE): Mission Description and Initial On-orbit Performance, AJ, 140, 1868
Yang, Q., Shen, Y., & Liu, X., et al. 2020, Dust Reverberation Mapping in Distant Quasars from Optical and Mid-Infrared Imaging Surveys, ApJ, 900, 58
Yu, Q. & Tremaine, S. 2002, Observational Constraints on Growth of Massive Black Holes, MNRAS, 335, 965